Underlying mechanism of shear-banding in soft glasses of charged colloidal rods with orientational domains

D. Parisi, D. Vlassopoulos, H. Kriegs, et al.

Citation: Journal of Rheology **66**, 365 (2022); doi: 10.1122/8.0000400
View online: https://doi.org/10.1122/8.0000400
View Table of Contents: https://sor.scitation.org/toc/jor/66/2
Published by the The Society of Rheology

Underlying mechanism of shear-banding in soft glasses of charged colloidal rods with orientational domains

D. Parisi,[1] D. Vlassopoulos,[1] H. Kriegs,[2] J. K. G. Dhont,[2] and K. Kang[2,a)]

[1]*Foundation for Research and Technology – Hellas (FORTH), Institute of Electronic Structure and Laser, GR-70013 Crete, Greece and Department of Materials Science and Technology, University of Crete, GR-71003 Crete, Greece*
[2]*IBI-4: Biomacromolecular Systems and Processes, Institute of Biological Information Processing, Forschungszentrum Jülich, Jülich 52428, Germany*

(Received 16 November 2021; final revision received 6 February 2022; published 24 February 2022)

Abstract

Soft glasses of colloidal rods (*fd*-virus particles) with orientational domains were recently shown to exhibit inhomogeneous flow profiles [Dhont *et al.*, Phys. Rev. Fluids **2**, 043301 (2017)]: fracture and accompanied plug flow at small shear rates, which transits to gradient shear-banding on increasing the shear rate, while a uniform flow profile develops at sufficiently high shear rates. These flow profiles coexist with Taylor-vorticity bands. The texture of such glasses under flow conditions consists of domains with varying orientations. The observed gradient shear-banding was solely attributed to the strong shear thinning behavior of the material inside the domains (henceforth abbreviated as domain-interior), without considering the texture stress that is due to interactions between the glassy domains. Here, we present new experiments on the shear-banding transition to assess the role played by the texture stress in comparison to the domain-interior stress. For a large concentration, well into the glassy state, it is found that both texture stress and domain-interior stress contribute significantly to the gradient shear-banding transition in the shear-rate region where it occurs. On the other hand, for a small concentration close to the glass-transition concentration, the domains are shown to coalesce within the shear-rate range where gradient shear-banding is observed. As a result, the texture stress diminishes and the domain-interior stress increases upon coalescence, leading to a stress plateau. Thus, a subtle interplay exists between the stresses arising from the structural order on two widely separated length scales from interactions between domains and from the rod-rod interactions within the domain-interior for both concentrations.
https://doi.org/10.1122/8.0000400

I. INTRODUCTION

Glasses of colloidal particles are long-lived metastable states, where collective rearrangements of the colloids with repulsive interactions, that would lead to equilibration, are hindered by the crowded environment of their neighbors. Contrary to such repulsive glasses, gels are long-lived non-equilibrium states due to strong attractive interparticle colloidal interactions, where the typical microstructural order consists of strings of physically interconnected particles. Mixed glass-gel states consist of colloidal particles with interaction potentials reflecting an appropriate combination of repulsive and attractive interactions (see [1] and [2]). Glasses of spherical colloids and many other types of complex fluids are known to exhibit shear-banding, where two regions (the "bands") with different shear rates coexist (see, for example, [3–13]). The classic scenario for shear-banding calls for strong shear thinning of the *homogeneously* sheared system such that the stress decreases with increasing shear rate. An early model predicts such a strong shear thinning behavior for glasses of spherical particles [14]. A decrease in the stress upon increasing the shear rate implies that a smaller force is needed to achieve a larger shear rate. This is counterintuitive and hints to instability [15,16]. It is indeed easily shown from the Navier–Stokes equation that a homogeneously sheared system for which the stress decreases with the increasing shear rate is unstable. Constitutive relations have been proposed that extend the standard relations to be able to describe the shear-banding transition. In those shear-banding phenomena where the bands consist of regions with different shear rates, these extensions are necessary to account for the large spatial gradients of the flow velocity within the "interfaces" that connect the shear bands. The standard Navier–Stokes equation can be extended to include such higher order gradient contributions by either adding a diffusive term to the equation of motion for the stress (the so-called "stress-diffusion contribution" [5,10]) or by adding higher order spatial derivatives directly to the stress tensor (the so-called "shear-curvature contribution" [11,12], for which a microscopic derivation for spherical colloids is given in [17]). A recent overview of such shear-banding constitutive equations where higher order spatial derivates are added to the constitute equation for a homogeneously sheared system can be found in [18]. These constitutive equations predict that the stable state in such cases exists of two "shear bands," within which the shear rate is constant. The corresponding stationary *inhomogeneously* sheared system, where the velocity shear bands are fully developed, exhibits

a)Author to whom correspondence should be addressed; electronic mail: k.kang@fz-juelich.de

a stress plateau. This scenario is present at the origin of shear-banding found in soft glasses of star polymers [19–22] and other types of systems with a yield stress such as gels [23,24], cement [25], and emulsions [26–28].

Other types of shear banding transitions are the result of coupling of the stress with an order parameter, like the orientational order parameter in liquid crystals (in the absence of a domain texture). Here, a coexistence between isotropic regions and aligned regions (the "bands") is found, which, however, requires higher order spatial gradients in the equation of motion for the order parameter. These are usually incorporated through a square-gradient expansion of the free energy that contributes to the equation of motion for the order parameter. Since the local orientation couples with the stress, the flow velocity also varies from one band to the other but in a less pronounced manner compared to the order parameter (see, for example, [29], where, contrary to our system, no orientational domain texture is present).

When compared to the systems mentioned above, much less is known about the glass transition and the flow behavior of glasses of long and thin colloidal rods. Glass transitions have been reported for systems of inorganic colloidal rods in [30] and for *fd*-virus particles at low ionic strength in [31], [32], [33], and [34]. *fd*-viruses are long and thin, highly charged, and stiff rodlike particles (see "Materials: Charged DNA-rods" section). At an ionic strength larger than about 1 mM, they exhibit a rich liquid-crystalline phase behavior (see, for example, [35–39]). In addition, a glass transition is only observed for ionic strengths less than about 1 mM [33], which is due to the relatively long-ranged electrostatic interactions corresponding to the low ionic strength, where the Debye length is much larger than the thickness of the cores of the rods. Here, we use *fd*-suspensions at an ionic strength of 0.16 mM (Tris/HCl buffer, at *p*H 6.8). The glass-transition concentration (∼11.7 mg/ml) is far above the isotropic-nematic upper-binodal concentration (∼3.4 mg/ml) where the system becomes fully chiral-nematic [31,32], with a typical chiral-nematic pitch of 50–500 μm, depending on the ionic strength and *fd*-concentration [40,41]. It is found that at the glass-transition concentration *both fd*-particle dynamics of the material inside the domains and the orientational-texture dynamics are arrested [31,32]. The morphology of glassy *fd*-suspensions, therefore, consists of randomly oriented domains. There are thus two contributions to the stress in such a system under flow conditions: the stress originating from the response of the material inside the domains (which we will hereafter refer to as the " domain-interior stress" for brevity) and the *texture stress* due to interactions between the glassy domains.

With "texture," we thus refer in the present study to the existence of chiral nematic polydomains [33,41]. Stresses induced by the response of disclinations, by a chiral-nematic structure, by flow-induced tumbling and wagging, and friction between domain boundaries, are all more generally referred to as "texture stress" [42–49]. The texture stress that includes all these contributions is shown, in [50], to be very small for *fd*-virus suspensions at much higher ionic strengths, where no rod-glass transition occurs. On the contrary, in the present study, we find that the domain-interior stress is of the same order of magnitude as the orientational-texture stress where tumbling and wagging are arrested and where, most probably, the degree of nematic alignment will not be significantly affected by the flow. In our case, the chiral-mesophase domains are elongated, where a distinction can be made concerning the kinetics of their formation in the two directions along and perpendicular to the direction of elongation in the absence of flow as observed by means of optical microscopy [41]. The domains behave as elastic entities due to their glassy content. The "texture stress" in the present study is, therefore, conjectured to be mainly the result of interactions between the elastic domains which flow past each other.

In our previous works [51,52], different nonuniform flow profiles were observed within the glassy state. At small applied shear rates, fracture and plug flow were detected, at an intermediate shear rate, there was a seemingly sharp transition to gradient shear-banding, while at high shear rates, a linear flow profile prevailed (see Fig. 2, which will be discussed in more detail below). All these flow profiles coexisted with Taylor-vorticity bands with a spatial extent that was much larger than the average domain size. The observed gradient shear-banding is attributed, in [51], to strong shear thinning behavior of the domain-interior once its corresponding yield stress was surpassed.

The purpose of the present study is to underpin the above conjecture with new systematic experiments, where the contribution from the texture stress is carefully investigated. Stress measurements are performed with small-volume (cone-plate geometry) and large-volume (Couette geometry) shear cells to distinguish between the separate contributions from the domain-interior and the domain texture to the total stress, respectively. The cone-plate geometry that is used has a spacing of 250 μm at the outer edge, while the typical domain size is of the order of sub-100–300 μm. Since at most a few domains are contained in such a small-volume geometry, and the domains merge under flow conditions in the confining geometry, the stress as measured with the cone-plate geometry probes predominantly the domain-interior stress. For the Couette cell that is used, with a gap width of 1 mm, many domains are present so that the texture stress contributes to the total stress. The difference between the two stress measurements, therefore, reveals the texture stress itself.

II. MATERIALS: CHARGED DNA-RODS

In this study, we use *fd*-virus particles as a model system for charged colloidal rods. Each rod consists of a double-stranded DNA covered with 2700 coat proteins, which confer a high negative charge of about 10 elementary charges per nm within a *p*H range of 5–9 [53]. The contour length of *fd*-virus particles is 880 nm, the width is 6.8 nm, corresponding to a bare aspect ratio of $p_b = 130$. The coat proteins render them a persistence length of about 2800 ± 700 nm [54]. Note that the *fd*-virus particles are identical so that the rod dispersions are strictly monodisperse. Since the persistence length is considerably larger than the contour length, these particles have been used as models for long, thin, and stiff colloidal rods. Here, we use a low ionic strength of 0.16 mM of TRIS/HCl buffer with $p\mathrm{H} = 6.8$, where the Debye length is 27 nm. The corresponding thick electric double layer results in an effective core

thickness of $D_{\text{eff}} = 27\,\text{nm}$, corresponding to an effective aspect ratio of $p_{\text{eff}} = 33$ [55]. As discussed in the Introduction, the long-ranged electrostatic interactions, where the Debye length is much larger than the core diameter, give rise to a glass transition at a *fd*-concentration of ~11.7 mg/ml. A schematic phase diagram for the given ionic strength of 0.16 mM in terms of the shear-rate ($\dot{\gamma}$) versus the *fd*-concentration ([fd]) is given in Fig. 1, based on data from [51], [33], [34], and [40]. In the absence of shear flow, there is an isotropic-nematic coexistence (indicated by I/N) for concentrations between 1.5 and 3.4 mg/ml, with chiral mesophases (indicated by $\tilde{N}^{\star}$) above the coexistence region, while the glass transition occurs far into the full nematic state. The dashed red line indicates where the domain texture disappears on increasing the shear rate. Gradient shear-banding occurs in the region between the blue lines, and Taylor-banding, where the bands are in internal rolling flow which are stacked along the vorticity direction, occurs in the region between the green lines. A linear flow profile is found within the shear-molten region, and above a shear rate of approximately $150\,\text{s}^{-1}$, where texture is still present for sufficiently high *fd*-concentration. As predicted by Onsager [55], the lower- and upper-binodal concentrations correspond to values of $(L/D)\varphi = 3.3$ and 4.2, respectively, for very long and thin rods, where φ is the volume fraction of *fd*-virus particles. The relation between the volume fraction φ_b of the bare cores of the rods and their weight concentration c, as obtained from the molar mass of *fd*-virus, reads $\varphi_b = 0.011\,c\,(\text{mg/ml})$. The effective values for $(L/D)\varphi$ (accounting for the increased value of the diameter of the rods due to electrostatic interactions), corresponding to the experimental lower- and upper-binodal concentrations, are thus equal to 0.9 and 2.0. These values are of the same order as those predicted by Onsager for rods with an infinite aspect ratio [55]. The full phase diagram in the absence of shear flow, where also the ionic strength is varied, which affects the effective aspect ratio, is discussed in [33].

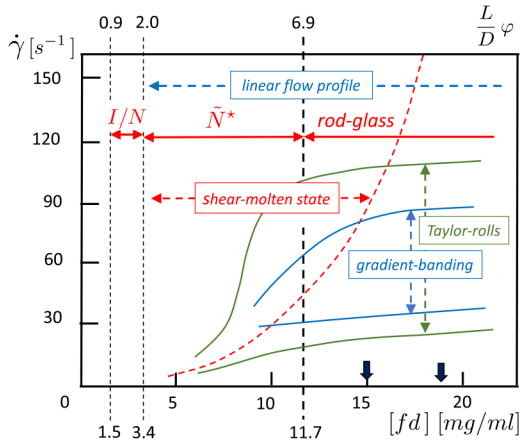

FIG. 1. A schematic phase diagram in the shear-rate versus concentration plane for an ionic strength of 0.16 mM. "I/N" for isotropic-nematic coexistence and "$\tilde{N}^{\star}$" stands for chiral-mesophases with different types of structural characteristics. The glass transition is located at 11.7 mg/ml, far above the upper binodal, concentration. The upper numbers are the effective values of $(L/D)\varphi$, as a comparison to predictions by Onsager for rods with an infinite aspect ratio. The two thick arrows on the concentration axis indicate the two concentrations where the experiments have been conducted.

III. EXPERIMENTAL METHODS: VELOCITY PROFILES AND SHEAR RHEOLOGY

Velocity profiles along the velocity-gradient direction were obtained by means of an optically transparent home-made cylindrical glass Couette cell with a 1 mm gap width, a diameter of the inner cylinder of 46 mm, and a minimum sample volume ~6 ml, using a spatially resolved heterodyne dynamic light scattering technique. A relatively small gap width is used to reduce the effects of shear-gradient induced migration of the colloidal particles [56]. Depending on the local flow velocity, this technique is operated in either the backscattering or the forward scattering configuration. Details about the experimental setup and analysis of the intensity autocorrelation functions are reported in [51] and [52]. The temperature was set to 22 °C and controlled by a thermal bath of silicon oil that matches the refractive index of the Couette cell connected to a water recirculating system. Steady-shear experiments were performed after thermal equilibration of the sample, lasting at least 20 min to establish stationary velocity profiles. The necessary long waiting times are due to the glassy nature of the samples. Flow profiles are averages of three repeated measurements.

Shear rheology experiments were performed on a sensitive strain-controlled ARES-HR rheometer (TA, USA), equipped with a force rebalance transducer 100FRTN1. We used two stainless steel measuring geometries: (i) a concentric cylindrical Couette cell with 1 mm gap width and an inner cylinder diameter of 46 mm to mimic the same conditions as the velocity profile measurements and (ii) a roughened 25 mm diameter cone and plate geometry with 0.02 rad cone angle and truncation equal to 23 μm. As mentioned before, the relatively small gap width for the Couette geometry is chosen to reduce shear-gradient induced migration [56]. Note that the maximum gap at the perimeter of the plate is 250 μm, four times smaller than the gap width of the concentric cylinders. As will be discussed below, this has a significant impact on the rheological response. The measuring time per shear rate to ensure steady state during the flow ramp was first determined via a start-up of shear rate at the lowest shear rate ($1\,\text{s}^{-1}$) and was found to be equal to 100 s. It follows that each point of the reported flow curves is at a steady state. Ascending and descending flow ramps were performed in the shear-rate range $1–150\,\text{s}^{-1}$. We note that in cone-plate geometry, edge effects can affect stress measurements and, in particular, lead to erroneous results for the yield stress in case edge effects are not accounted for [57,58]. Corroborating this point, in our measurements, we apply shear rates where the stress is significantly larger than the yield stress and possible edge effects are negligible.

IV. RESULTS AND DISCUSSION

Gradient shear-banded velocity profiles for *fd*-concentrations of 19 and 15 mg/ml, above the glass-transition concentration of $11.7 \pm 0.6\,\text{mg/ml}$ (for the ionic strength of 0.16 mM Tris/HCl buffer) are depicted in Fig. 2, where the applied shear rates vary from 36 to $150\,\text{s}^{-1}$. Here, the position of 0 mm corresponds to the stationary outer cylinder, while 1 mm is the position of the

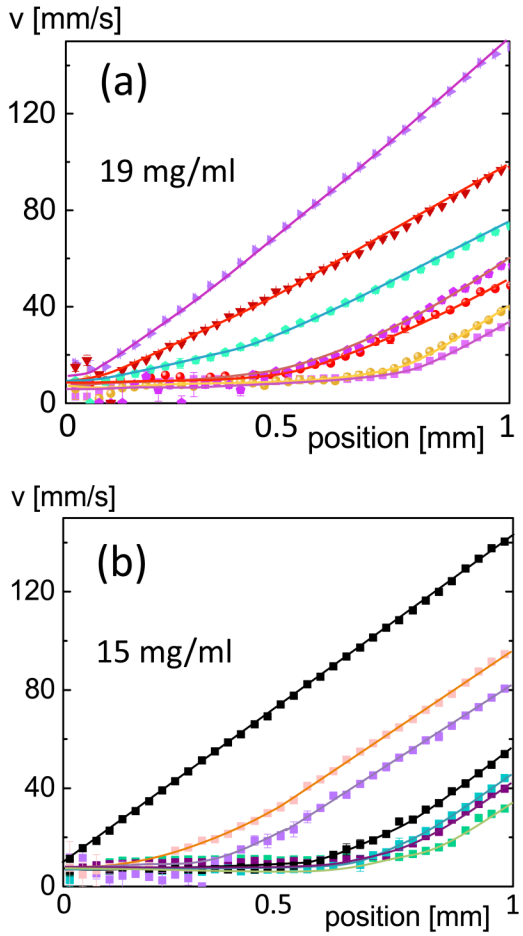

FIG. 2. Velocity profiles for a *fd*-virus concentration of (a) 19 mg/ml and (b) 15 mg/ml at 22 °C in a 1 mm gap width Couette cell for shear rates, from bottom to top, 36, 46, 50, 60, 85, 100, and 150 s^{-1}. Solid lines are various shear rates a guide for the eye. The position zero coincides with the stationary outer cylinder, whereas the position at 1 mm represents the rotating inner cylinder.

rotating outer cylinder. The velocity profile measurements were performed under controlled shear rate conditions so that at least part of the sample was fluidized, that is, in at least part of the sample, the local stress was larger than the local yield stress. Two shear bands are found: a band at the stationary outer cylinder (position 0 mm) where the shear rate is essentially equal to zero and a band at the rotating cylinder (position 1 mm) with a nonzero shear rate. As can be seen in Fig. 2, the shear rate within the latter band is constant, equal to $\sim 80\,s^{-1}$ for 19 mg/ml and $\sim 130\,s^{-1}$ for 15 mg/ml, independent of the applied shear rate. Such a constant shear rate resembles an ideal gradient shear-banding scenario [5,6,12].

The reason for choosing a Couette geometry with a relatively small gap width is to reduce the spatial gradients in the shear rate, which could induce mass transport (for the chosen geometry, the shear rate varies from the inner to the outer cylinder by about 2%). Our experimental results show that the extent of the low-shear-rate branch continuously decreases with increasing applied shear rates, leading to a linear flow profile for sufficiently large shear rates. These results are in accordance with those in [51] and [52] and have been observed both close to the glass transition and well within the glassy state.

In order to verify that the shear-banded profiles are indeed connected to the classic gradient-banding scenario, measurements of the shear stress as a function of the applied shear rate were performed. As discussed in the Introduction, within the classic gradient shear-banding scenario, banding is due to very strong shear thinning of the *homogeneously* sheared system such that the total shear stress decreases with an increase in the shear rate. In the stationary state, where the system is *inhomogeneously* sheared, a shear-stress plateau is revealed, i.e., the shear stress is independent of the applied shear rate (for relevant overviews on shear-banding, see, for example, [5], [6], [7], and [12]). A slight inclination is sometimes observed due to different microstructural orders or concentrations within the two bands) [8,19]. Such a stress plateau has been observed from measurements with a cone-plate geometry in [51], with spatial dimensions that are less than the average size of single domains (the domain size is in the range sub-100–300 μm) [33]. For such small volumes in the cone-plate geometry, in which just a few domains can be present, the texture stress arising from interactions between domains is essentially absent. The observed gradient shear-banding was attributed, in [51], to the strong shear thinning behavior of the material inside single domains, that is, the *domain interior*. However, for the optical Couette cell with a gap width of 1 mm used for the velocity measurements, with which the gradient shear-banded flows given in Fig. 2 are observed, an orientational texture consisting of many domains is present [31,32]. The question thus arises here is what is the role the texture shear-stress plays in the mechanism leading to the observed gradient shear-banded flow in the Couette geometry.

Flow curves (shear stress under controlled shear-rate conditions as a function of the externally applied shear rate) for a relatively large concentration of 19 mg/ml are given in Fig. 3 [in Fig. 3(a) on a log scale for the shear rate and in Fig. 3(b) on a linear scale, in order to emphasize the small and large shear rates regimes, respectively). The vertical red dashed lines mark the region where the stress plateau is seen. The red dashed line that marks the upper shear rate is smaller than the shear rate where shear banding is seen in Fig. 2. This is most probably due to a slip. The indicated shear rates relating to the flow curves are hereafter the applied shear rates. The reason for the differences in the slip between the shear cells is unclear. That the stationary state is probed during measurements is supported by the proximity of measured stress data upon decreasing and increasing the applied shear rate (the open and solid symbols in Fig. 3, respectively), as well as transient measurements during which the stationary is reached. The blue symbols in Fig. 3 are data obtained with the Couette cell and the red data points with the cone-plate geometry. Since essentially no texture is present in the cone-plate geometry, the significant difference between the two sets of data points is attributed to the texture stress, which measures, roughly, the product of the texture density (the number of interfaces per unit area that cross the velocity-gradient plane) multiplied by the stress due to a single texture interface. Such an interpretation is only valid in case the flow profiles in both geometries are the same in the sense that two shear bands are present with the same relative spatial extent. This is guaranteed by the observation that shear banding

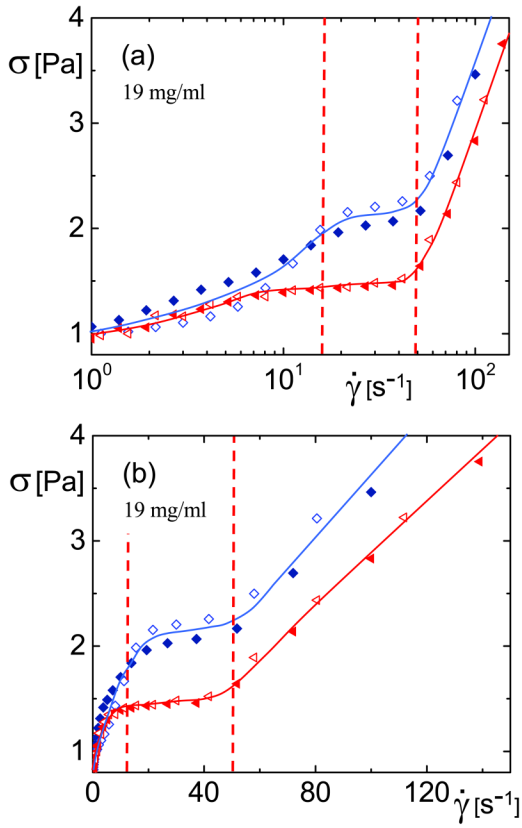

FIG. 3. Flow curves in terms of shear stress σ as a function of shear rate $\dot{\gamma}$ for the *fd*-virus solution at 19 mg/ml at 22 °C obtained from experiments either with the 1 mm gap width Couette geometry (blue diamonds) or roughened 25 mm diameter cone-plate geometry (red triangles). Panel (a) is on linear-logarithmic scale, whereas panel (b) on linear-linear scale, in order to emphasize the behavior at small- and large shear-rates. The solid symbols are data obtained by sequentially increasing the shear rate and the open symbols by decreasing the shear rate. The vertical (red) dashed lines mark the region where the stress plateau is seen.

occurs in both geometries in the same shear rate range (as evidenced by the flow curves in Fig. 3), and the fact that the extent of the bands is determined by the geometry-independent stress-selection rule together with the van der Waals looplike form of the constitutive relation for the homogeneously sheared

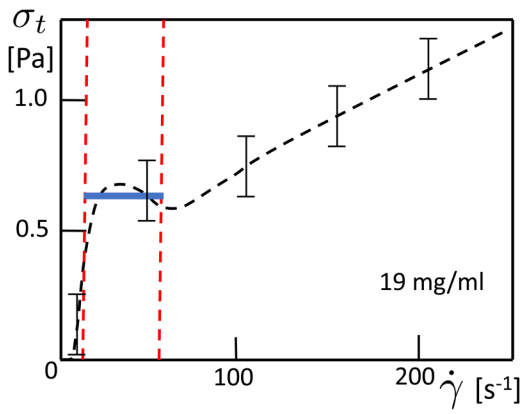

FIG. 4. The texture stress σ_t for a large *fd*-concentration of 19 mg/ml as a function of the shear rate. The dashed curve is the difference between the blue and red curves in Fig. 3, on which the error bars as indicated are based. Within the shear-rate region where gradient shear-banding is observed, the texture stress is basically constant, independent of the shear rate within the experimental error, as indicated by the thick (blue) line. The vertical (red) dashed lines mark the region where the stress plateau is seen.

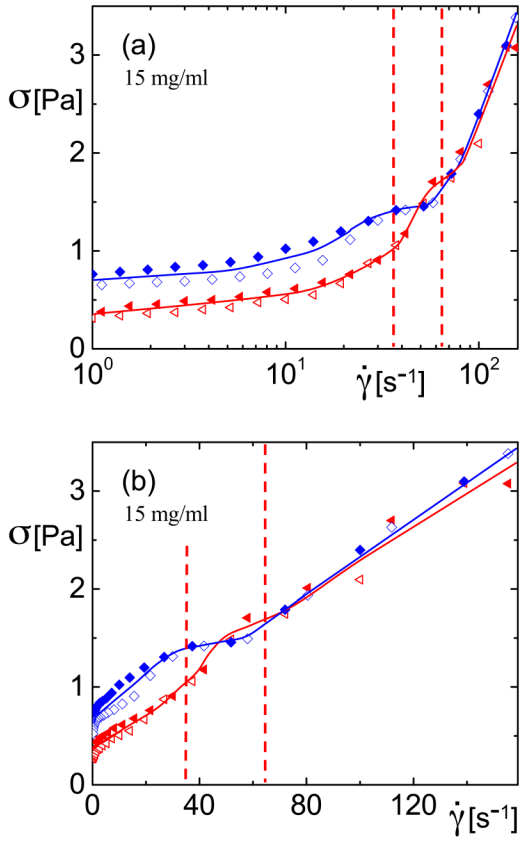

FIG. 5. Flow curves in terms of shear stress σ as a function of shear rate $\dot{\gamma}$ for the *fd*-virus solution with a concentration of 15 mg/ml at 22 °C with symbols the same as in Fig. 3.

system. Henceforth, we will, therefore, refer to the difference between the stress obtained with the Couette cell and the cone-plate geometry as "the texture stress" σ_t. It should be mentioned, however, that the texture stress thus defined is affected by the domain-interior stress and vice versa, as will be seen later. The thus obtained texture stress σ_t is plotted in Fig. 4. The average of the data points upon increasing and decreasing the shear is used here because the hysteresis is attributed to the not fully adapted structural order on either increasing or decreasing the shear rate. The true stress, corresponding to the newly applied shear rate, is expected to lie in between the two sets of open and solid data points. As can be seen, the data corresponding to the shear response of single domains (which reproduces earlier measurements for a similar concentration in [51]) show the expected stress plateau. However, the stress arising from the domain texture is of the same order as that of the domain-interior. In order to produce a stress plateau for the total stress, the texture stress must, therefore, exhibit a stress plateau by itself. Figure 4 shows that this is indeed the case. The conclusion is that for this large concentration of 19 mg/ml, well into the glass state, the shear stresses both from the domain-interior as well as the texture stress are responsible for the existence of gradient banded flows. There is thus a subtle interplay between the shear response of the domain-interior and that of the texture. The response of both is interrelated since changes in the domain interior affect the interactions between the domains, and *vice versa*, forces onto domains due to domain interactions affect the domain-interior.

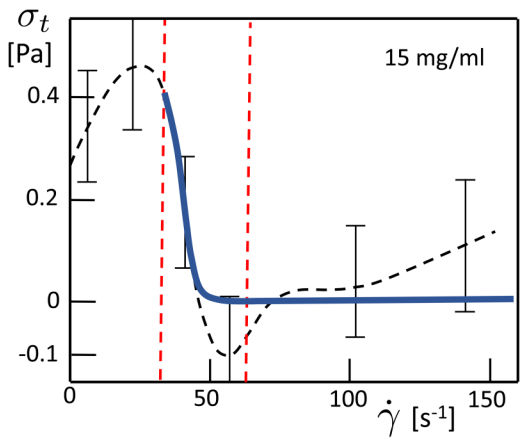

FIG. 6. The texture stress σ_t for a *fd*-concentration of 15 mg/ml as a function of the shear rate. The symbols are the same as in Fig. 4. Within the shear-rate region where gradient shear banding is observed, the texture stress diminishes due to the coalescence of the domains, as indicated by the thick (blue) curve.

The situation for an *fd*-concentration of 15 mg/ml (corresponding to a weaker glass) is different, and revealing of this subtle interplay, as shown in Fig. 5. As before, the red curve corresponds to the total stress as obtained with the Couette cell, while the red curve reflects the response of the domain-interior as measured with the cone-plate geometry. The difference between the curves thus reflects again the contribution from the texture stress σ_t, which is plotted in Fig. 6. The measured stresses with the Couette cell and the cone-plate geometry coincide above an applied shear rate of about 50 s^{-1}, which is located within the shear-rate range where banding occurs (see the two red dashed lines in Figs. 5 and 6). This implies that in this case, the (majority of the) domains have merged (coalesced) and, essentially, no distinct texture is present as also inferred by the fact that there is a negligible contribution from the texture stress. As can be seen from the blue curve in Fig. 6, where the texture stress σ_t is plotted as a function of the shear rate, the texture stress diminishes at first due to the merging of the domains within the banding region, and, subsequently, it vanishes to within experimental error. As can be seen from Fig. 5, the coalescence of the domains leads to an increase in the stress from the domain-interior, which compensates the concomitant diminishing texture stress such that the total stress exhibits a stress plateau.

The existence of domain texture for 19 mg/ml and its virtual disappearance at 15 mg/ml for a shear rate of 75 s^{-1} (just beyond the shear rate where the texture stress for the small *fd*-concentration vanishes, as can be seen in Fig. 6) is verified by direct visual observation. The images in Fig. 7 are side-views of the optical Couette cell, where the vertical direction is the vorticity direction and the horizontal direction corresponds to the flow direction. The images show the full extent of the Taylor-vorticity rolls of spatial extent 3.7 mm, with which the gradient banded flows coexist. The much more frequent spatial variation of the intensity of the image for the large concentration due to the existence of a domain texture as compared to the small concentration is confirmed by the intensity profiles on the left and right in Fig. 7. Note that the images are a superposition of the texture extending throughout the cell gap in the gradient direction, which tends to blur them to some extent.

The hysteresis of the stress in the Couette cell is systematically larger than in the cone-plate fixture, which implies that the texture relaxes to the stationary state on a longer time scale as compared to the domain interior. The most probable reason for this is that changes of the texture require structural rearrangements on a much larger length scale than for the domain-interior. Note that within experimental error, there is no hysteresis for large shear rates beyond the banding regime for the low concentration of 15 mg/ml. The most probable reason is that for this concentration, there is no texture present anymore for these large shear rates. Note that there is a switching of hysteresis in Fig. 3 for high concentrations at the shear rate where on decreasing the shear rate, banding ceases to occur. It is currently unclear what the mechanism behind this switch is.

These experiments show that for large concentrations, well inside the glassy regime, where domains are expected to be relatively rigid, the texture stress contributes equally to the total stress as compared to the stress due to the domain-interior, contrary to what was conjectured in [51] where only the latter contribution was considered. Both domain-interior stress and texture stress exhibit a stress plateau within the shear-rate range where gradient shear-banding occurs. For

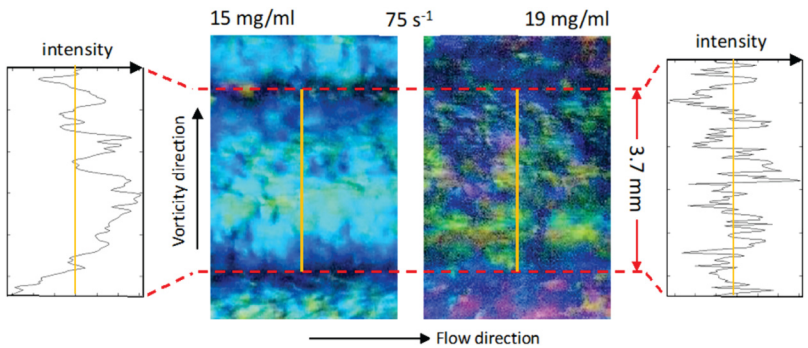

FIG. 7. Images of the morphology were taken from the side of the optical Couette cell for 15 mg/ml (left panel) and 19 mg/ml (right panel) at a shear rate of 75 s^{-1}. The two red dashed lines indicate the extent of a Taylor-vorticity band, the height of which is 3.7 mm. The intensity profiles on the left and right show the recorded intensity of single camera pixels in the middle of the images as a function of the position along the vorticity direction (as indicated by the vertical yellow lines in the two images). The images are processed from Fig. 12 in [52].

small concentrations, however, the less rigid domains coalesce within the shear-banding regime such that the total stress exhibits a stress plateau.

V. SUMMARY AND CONCLUSIONS

We have performed velocity profile and shear rheology measurements which, complemented by optical microscopy imaging from the literature, elucidate the underlying complex mechanism for the existence of nonuniform flow profiles in soft glasses of long and thin, charged colloidal rods (*fd*-virus particles) [51,52]. For these glasses, it is found that both *fd*-particle dynamics inside domains and the dynamics of the domain texture are arrested at the same glass-transition concentration of $11.7 \pm 0.6\,\mathrm{mg/ml}$, far above the isotropic-nematic coexistence region [31,32]. The following distinct flow profiles are observed: (i) plug flow and fracture at small applied shear rates (which has been observed in [51] and [52]), (ii) gradient shear-banding profiles at intermediate shear rates, and (iii) a linear profile at sufficiently high shear rates. It should be noted that these flow profiles coexist with Taylor-vorticity bands [51,52].

One of the scenarios for gradient shear-banding is strong shear thinning of the *homogeneously* sheared material at hand, which leads to a stress plateau in the stationary state, once an inhomogeneous shear-banded flow profile is fully developed. The observed gradient shear-banding for the charged colloidal rod-glass was attributed, in [51], to the strong shear thinning behavior of the domain-interior. Here, in addition to complementary velocimetry, the stress was measured as a function of the applied shear rate in the stationary state (referred to as a flow curve). We used a cone-plate geometry with sufficiently small spatial dimensions such that at most a few domains are present within the shear cell and a cylindrical Couette fixture whose gap encompasses many domains. In the cone-plate shear cell, the stress response of the domain-interior is probed. In the Couette shear cell, the texture stress due to interactions between domains contributes to the rheological response as well. On the basis of the following observations, it is concluded in the present study that both domain-interior and texture stress due to interactions between domains are at the origin of the shear-banded flow profiles.

- For large concentrations, well into the glassy regime, the flow curve as obtained with the Couette cell shows the expected stress plateau for the total stress. The flow curve obtained with the cone-plate geometry shows that the stress arising from the domain-interior also exhibits the same stress plateau within the same shear-rate range. The texture stress and the stress from the domain-interior are of the same order of magnitude. This shows that both stress contributions are responsible for the observed gradient shear-banded flow profiles. For this large concentration, the domain texture remains intact for all applied shear rates.
- For the small concentration closer to the glass-transition concentration, corresponding to a weaker glass, the texture stress diminishes and, in fact, vanishes in the shear-rate range where gradient shear-banding is observed, while the stress of the domain-interior increases. Direct observation of the texture confirms that the domains coalesce, leading to the disappearance of the domain texture. The combination of the two stress contributions leads to a stress plateau that is associated with shear-banding, as revealed by velocity measurements.

Contrary to nonglassy systems of nematic *fd*-virus suspensions, where the texture stress is negligible [50], the texture stress in the glassy state is found to be of the same order of magnitude as the domain-interior stress. Within the classic banding scenario, the total stress (being equal to the sum of the domain-interior stress and the texture stress) exhibits a stress plateau in the stationary shear-banded state. Here, we find that both of these separate contributions exhibit such a stress plateau, which implies that there is a subtle interplay between the interdomain- and texture-stress responses. The interactions between the domains affect their internal structure, which, in turn, affects the interactions between the domains.

The formation of glass depends critically on the ionic strength: a glassy state does not exist for ionic strengths larger than about 0.8 mM and lower than 0.1 mM. The rheological response of *fd*-rod glasses may, therefore, be quite sensitive to the ionic strength, which is not addressed in the present study. An equilibrium phase diagram for this system, including the glass state, in the *fd*-concentration versus ionic-strength plane, for low ionic strengths, can be found in [33]. Furthermore, it would be interesting to perform 3D-imaging experiments under flow conditions to determine the domain-size distribution within the shear bands. It might well be that there is a different size distribution within the two shear bands.

ACKNOWLEDGMENTS

Part of the experiments has been performed with financial support from the European Union's Horizon 2020 Research and Innovation Programme (EUSMI) under Grant Agreement No. 731019.

REFERENCES

[1] Solomon, M. J., and P. T. Spicer, "Microstructural regimes of colloidal rod suspensions gels, and glasses," Soft Matter **6**, 1391–1400 (2010).
[2] Zaccarelli, E., and W. C. K. Poon, "Colloidal glasses and gels: The interplay of bonding and caging," Proc. Natl. Acad. Sci. U.S.A. **106**, 15203–15208 (2009).
[3] Fielding, S. M., "Complex dynamics of shear banded flows," Soft Matter **3**, 1262–1279 (2007).
[4] Callaghan, P. T., "Rheo NMR and shear banding," Rheol. Acta **47**, 243–255 (2008).
[5] Olmsted, P. D., "Perspectives on shear banding in complex fluids," Rheol. Acta **47**, 283–300 (2008).
[6] Manneville, S., "Recent experimental probes of shear banding," Rheol. Acta **47**, 301–318 (2008).
[7] Schall, P., and M. van Hecke, "Shear bands in matter with granularity," Annu. Rev. Fluid Mech. **42**, 67–88 (2010).
[8] Fielding, S. M., and P. D. Olmsted, "Flow phase diagrams for concentration-coupled shear banding," Eur. Phys. J. E **11**, 65–83 (2003).

[9] Divoux, T., M. A. Fardin, S. Manneville, and S. Lerouge, "Shear banding of complex fluids," Ann. Rev. Fluid Mech. **48**, 81–103 (2016).
[10] Helgeson, M. E., P. A. Vasquez, E. W. Kaler, and N. J. Wagner, "Rheology and spatially resolved structure of cetyltrimethylammonium bromide wormlike micelles through the shear banding transition," J. Rheol. **53**, 727–756 (2009).
[11] Dhont, J. K. G., "A constitutive relation describing the shear-banding transition," Phys. Rev. E **60**, 4534–4544 (1999).
[12] Dhont, J. K. G., and W. J. Briels, "Gradient and vorticity banding," Rheol. Acta **47**, 257–281 (2008).
[13] Burroughs, M. C., Y. Zhang, A. M. Shetty, Ch. M. Bates, L. G. Leal, and M. E. Helgeson, "Flow-induced concentration nonuniformity and shear banding in entangled polymer solutions," Phys. Rev. Lett. **126**, 207801 (2021).
[14] Coussot, P., and G. Ovarlez, "Physical origin of shear-banding in jammed systems," Eur. Phys. J. E **33**, 183–188 (2010).
[15] McLeish, T. V. B., and R. C. Ball, "A molecular approach to the spurt effect in polymer melt flow," J. Polym. Sci., Part B: Polym. Phys. **24**, 1735–1745 (1986).
[16] Cates, M. E., T. C. B. McLeish, and G. Marrucci, "The rheology of entangled polymers at very high shear rates," Eur. Phys. Lett. **21**, 451–456 (1993).
[17] Jin, H., K. Kang, K. H. Ahn, W. J. Briels, and J. K. G. Dhont, "Non-local stresses in highly non-uniformly flowing suspensions: The shear-curvature viscosity," J. Chem. Phys. **149**, 014903 (2018).
[18] Lerouge, S., and P. D. Olmsted, "Non-local effects in shear banding of polymeric flows," Front. Phys. **7**, 246 (2020).
[19] Holmes, W. M., P. T. Callaghan, D. Vlassopoulos, and J. Roovers, "Shear banding phenomena in ultrasoft colloidal glasses," J. Rheol. **48**, 1085–1102 (2004).
[20] Rogers, S. A., D. Vlassopoulos, and P. T. Callaghan, "Aging, yielding, and shear banding in soft colloidal glasses," Phys. Rev. Lett. **100**, 128304 (2008).
[21] Beris, A. N., E. Stiakakis, and D. Vlassopoulos, "A thermodynamically consistent model for the thixotropic behavior of concentrated star polymer solutions," J. Non-Newtonian Fluid Mech. **152**, 76–85 (2008).
[22] Rogers, S. A., P. T. Callaghan, G. Petekidis, and D. Vlassopoulos, "Time-dependent rheology of colloidal star glasses," J. Rheol. **54**, 133–158 (2010).
[23] Moller, P. C. F., S. Rodts, M. A. J. Michels, and D. Bonn, "Shear banding and yield stress in soft glassy materials," Phys. Rev. E **77**, 041507 (2008).
[24] Fall, A., J. Paredes, and D. Bonn, "Yielding and shear banding in soft glassy materials," Phys. Rev. Lett. **105**, 225502 (2010).
[25] Jarny, S., N. Roussel, S. Rodts, F. Bertrand, R. Le Roy, and P. Coussot, "Rheological behavior of cement pastes from MRI velocimetry," Cem. Concr. Res. **35**, 1873–1881 (2005).
[26] Becu, L., S. Manneville, and A. Colin, "Yielding and flow in adhesive and nonadhesive concentrated emulsions," Phys. Rev. Lett. **96**, 138302 (2006).
[27] Ragouilliaux, A., G. Overlaz, N. Shahidzadeh-Bonn, B. Herzhaft, T. Palermo, and P. Coussot, "Transition from a simple yield-stress fluid to a thixotropic material," Phys. Rev. E **76**, 051408 (2007).
[28] Malkin, A. Y., and V. G. Kulichikhin, "Structure and rheology of highly concentrated emulsions: A modern look," Russ. Chem. Rev. **84**, 803–825 (2015).
[29] Marenduzzo, D., E. Orlandini, and J. M. Yeomans, "Interplay between shear flow and elastic deformations in liquid crystals," J. Chem. Phys. **121**, 582–591 (2004).
[30] Wierenga, A., A. P. Philipse, and H. N. W. Lekkerkerker, "Aqueous dispersions of colloidal Boehmite: Structure, dynamics, and yield stress of rod gels," Langmuir **14**, 55–65 (1998).
[31] Kang, K., and J. K. G. Dhont, "Glass transition in suspensions of charged rods: Structural arrest and texture dynamics," Phys. Rev. Lett. **110**, 015901 (2013).
[32] Kang, K., and J. K. G. Dhont, "Structural arrest and texture dynamics in suspensions of charged colloidal rods," Soft Matter **9**, 4401–4411 (2013).
[33] Kang, K., "Equilibrium phase diagram and thermal responses of charged DNA-virus rod-suspensions at low ionic strength," Sci. Rep. **11**, 3472 (2021).
[34] Kang, K., "Glass transition of repulsive charged rods (fd-viruses)," Soft Matter **10**, 3311–3324 (2014).
[35] Fraden, S., "Phase transitions in colloidal suspensions of virus particles," in *Observation, Prediction and Simulation of Phase Transitions in Complex Fluids*, NATO-ASI-Series C Vol. 460, edited by M. Baus, L. F. Rull, and J. P. Ryckaert (Kluwer Academic, Dordrecht, 1995), p. 113.
[36] Dogic, Z., and S. Fraden, "Cholesteric phase in virus suspensions," Langmuir **16**, 7820–7824 (2000).
[37] Grelet, E., and S. Fraden, "What is the origin of chirality in the cholesteric phase of virus suspensions?," Phys. Rev. Lett. **90**, 198302 (2003).
[38] Dogic, Z., and S. Fraden, "Phase behavior of rod-like viruses and virus-sphere mixtures," in *Soft Matter, Volume 2: Complex Colloidal Suspensions*, edited by G. Gompper and M. Schick (Wiley-VCH, Weinheim, 2006).
[39] Grelet, E., and R. Rana, "From soft to hard rod behavior in liquid crystalline suspensions of sterically stabilized colloidal filamentous particles," Soft Matter **12**, 4621–4627 (2016).
[40] Kang, K., "Chiral glass of charged DNA rods, cavity loops," J. Phys. Commun. **5**, 065001 (2021).
[41] Kang, K., "Characterization of orientation correlation kinetics: Chiral-mesophase domains in suspensions charged DNA-rods," J. Phys. Commun. **6**, 015001 (2022).
[42] De' Neve, T., P. Navard, and M. Kléman, "Shear rheology and shear-induced textures of a thermotropic copolyesteramide," J. Rheol. **37**, 515–529 (1993).
[43] Vermant, J., P. Moldenaers, S. J. Picken, and J. Mewis, "A comparison between texture and rheological behavior of lyotropic liquid crystalline polymers during flow," J. Non-Newtonian Fluid Mech. **53**, 1–23 (1994).
[44] Larson, R. G., "On the relative magnitudes of viscous, elastic and texture stresses in liquid crystalline PBG solutions," Rheol. Acta **35**, 150–159 (1996).
[45] Vermant, J., P. Moldenaers, S. J. Picken, and J. Mewis, "A comparison between texture and rheological behaviour of lyotropic liquid crystalline polymers during flow," J. Non-Newtonian Fluid Mech. **53**, 1–23 (1994).
[46] Larson, R. G., and M. Doi, "Mesoscopic domain theory for textured liquid crystalline polymers," J. Rheol. **35**, 539–563 (1991).
[47] Marrucci, G., "Rheology of liquid crystalline polymers," Pure Appl. Chern. **57**, 1545–1552 (1985).
[48] Kawaguchi, M. N., and M. M. Denn, "A mesoscopic theory of liquid crystalline polymers," J. Rheol. **43**, 111–124 (1999).
[49] Walker, L. M., and N. J. Wagner, "Rheology of region I flow in a lyotropic liquid-crystal polymer: The effects of defect texture under shear and during relaxation," J. Rheol. **38**, 1525–1547 (1994).
[50] Lettinga, M. P., Z. Dogic, H. Wang, and J. Vermant, "Flow behavior of colloidal rodlike viruses in the nematic phase," Langmuir **21**, 8048–8057 (2005).
[51] Dhont, J. K. G., K. Kang, H. Kriegs, O. Danko, J. Marakis, and D. Vlassopoulos, "Nonuniform flow in soft glasses of colloidal rods," Phys. Rev. Fluids **2**, 043301 (2017).

[52] Kang, K., "Response of shear in bulk orientations of charged DNA rods: Taylor- and gradient-banding," J. Phys. Commun. **5**, 045011 (2021).

[53] Zimmermann, K., H. Hagedorn, C. C. Heuck, M. Hinrichsen, and H. Ludwig, "The ionic properties of the filamentous bacteriophages Pfl and fd," J. Biol. Chem. **261**, 1653–1655 (1986).

[54] Barry, E., D. Beller, and Z. Dogic, "A model liquid crystalline system based on rodlike viruses with variable chirality and persistence length," Soft Matter **5**, 2563–2570 (2009).

[55] Onsager, L., "The effects of shape on the interaction of colloidal particles," Ann. N. Y. Acad. Sci. **51**, 627–659 (1949).

[56] Macosko, C. W., *Rheology: Principles, Measurements and Applications* (VCH, New York, 1994).

[57] Zhang, X., E. Lorenceau, P. Basset, T. Bourouina, F. Rouyer, J. Goyon, and P. Coussot, "Wall slip of soft-jammed systems: A generic simple shear process," Phys. Rev. Lett. **119**, 208004 (2017).

[58] Sharma, V., A. Jaishankar, Y.-C. Wang, and G. H. McKinley, "Rheology of globular proteins: Apparent yield stress, high shear rate viscosity and interfacial viscoelasticity of bovine serum albumin solutions," Soft Matter **7**, 5150–5160 (2011).